

RESEARCH PAPER

Control Optimization of a Dual-Stage Cable Robot with Redundancy Using State Dependent Riccati Equation Approach

Mohsen Nourizadeh¹, Moharram Habibnejad Korayem², Hami Tourajizadeh^{3,*}

Received 20 October 2024; Revised 15 December 2024; Accepted 20 January 2025;
© Iran University of Science and Technology 2025

ABSTRACT

The purpose of this paper is to optimal control a dual-stage cable robot in a predefined path and to determine the maximum load-carrying capacity of this robot as a tower crane. Also, to expand the workspace of the robot two stages are employed. Today, cable robots are extensively used in load handling. Positive cable tension and collision-free cable control are the most important challenges of this type of robot. The high ratio of transposable loads to weight makes these robots very attractive for use as tower cranes. Dynamic Load Carrying Capacity (DLCC) is the maximum load that can be carried along a predefined path without violating the actuators and allowable accuracy constraints. State-Dependent Riccati Equation (SDRE) is employed to control the end-effector within the path to achieve the maximum DLCC. This approach is chosen since it can optimize the required motors' torque which consequently leads us to the maximum DLCC. In addition, the constraint of cables' collision together is also checked along the predetermined path using the non-interference algorithm. The correctness of modeling is verified by comparing the results with previous research and the efficiency of the proposed optimal controlling strategy toward increasing the DLCC is investigated by conducting some comparative simulations. It is shown that the proposed cable robot by the aid of the designed optimal controller can increase the load carrying capacity successfully along any desired path using the allowable amount of motors' torque.

KEYWORDS: Dual-stage cable robot; Dynamic load carrying capacity (DLCC); State-dependent riccati equation (SDRE); Optimal control.

1. Introduction

The use of cable-driven robots is associated with advantages such as lower weight, bigger dynamic workspace, higher portable load to robot weight ratio, easier installation and maintenance, and faster performance and movements; Therefore, its application has become increasingly popular. The controllability-related discussions of cable robots have special importance due to the structural differences between cable robots and linkage ones and also due to the complexity and nonlinearity of their dynamic equations. Since the actuators of this robot is cable based, the efficient workspace of the robot is limited to the movements for which the cables' tension are positive. Also, the same as other parallel robots, the accessible dynamic workspace for such robots is completely dependent on the dimensions and configuration of the engaged platforms. The design of the first crane using six cables to suspend a pallet was made

by the National Institute of Standards and Technology (NIST) called Robocrane imitating the Stewart mechanism. The crane was operated manually using a Joy Stick and its purpose was to control or eliminate the unwanted oscillations of the load during landing and to control the destructive effects of the wind. Due to the strengths of this structure, cable robots can be employed in helicopter or balloon transfer, machining and shaping operations, drilling [1]. Cable robots are structurally divided into two categories: restricted (CRPM) and unrestricted (IRPM). Due to the structure and type of cables and the possibility of their collision with obstacles, CRPM robots are not used for transporting and handling the loads and docking, instead, robots with IRPM structures are used for this purpose. In these robots, the end-effector weight and its related load are themselves involved in providing the required tension of the cables [2]. Agrawal et al. developed the

* Corresponding author: Tourajizadeh Hami
Tourajizadeh@khu.ac.ir

1. Robotic Research Laboratory, Center of Excellence in Experimental Solid Mechanics and Dynamics, School of Mechanical Engineering, Iran University of Science and Technology, Tehran, Iran
2. Robotic Research Laboratory, Center of Excellence in Experimental Solid Mechanics and Dynamics, School of Mechanical Engineering, Iran University of Science and Technology, Tehran, Iran

3. Mechanical Engineering Department, Faculty of Engineering, Kharazmi University, Tehran, Iran

kinematics and dynamics of a cable robot and designed a linearized feedback controller for a six-degree-of-freedom space cable robot [3]. Agrawal team also analyzed the working space of this robot. The allowable workspace of the robot is a subset of the accessible space for the robot in which the traction of the cables is positive [4]. Other activities related to this group in this field include the study of the dynamics and control of docking and load handling by a six-degree-of-freedom cable robot connected to a helicopter. They proposed two slow and fast modes for independent control of the robot and the helicopter. In this regard, they were able to calculate the inputs of fast and slow-motion controllers of the helicopter by solving several nonlinear algebraic equations in each time interval [5]. Ji et al. studied an eight-DOF redundant cable robot and controlled the system using the cables' length feedback and a non-optimal sliding mode controller. The length of the cables is determined by taking feedback from the cable length sensors, and the actual position of the operator is calculated online using direct kinematic equations. Cable tension is assumed to be positive and workspace restrictions are not considered. Direct kinematic solution methods are based on the Tetrahedron approach and the Levenberg–Marquardt methods without analyzing the robot workspace [6]. Due to the large changes in the dynamic parameters of the cable robot and to increase the accuracy of tracking, Gouttefarde et al. designed and applied an adaptive dual-space motion control scheme for CDP. The proposed method aims at increasing the robot tracking performances while keeping all the cables tensed despite changes in robot dynamic parameters [7]. For the 6-cable-driven robot, whose two cables are parallel to each other, Gosselin et al. [8], analyzed the allowable workspace, accessible space, and its related singular points using an analytic approach. For the cables to be parallel in pairs, both cables must be driven by one motor, so this robot needs 3 motors; thereby, this reduces the costs and complexity of the work. On the contrary, this robot has three degrees and can only provide translational movement of the end-effector. All these activities are fulfilled for single-stage robots while the load-carrying capacity of the robot has not been also considered. Regarding the determination of the load-carrying capacity (DLCC) for cable robots, Korayem

et al. studied and developed the maximum dynamic load-carrying capacity for space cable robot (ICaSbot) using the variation method. The maximum load-carrying capacity was evaluated based on two restrictions including the output motors' torque and the maximum allowable error. In this study, the controller is an open loop, the cables and joints are assumed to be rigid, and the traction is assumed to be positive in the cables. In the simulation, the results of the maximum load-carrying capacity for the optimized predetermined path with an open-loop controller are presented [9]. Afterward, Korayem et al. developed a closed-loop controller for the cable, and the DLCC of ICaSbot was extracted for the closed-loop system using the same restrictions, and the results were compared to open open-loop case. Moreover, an algorithm was proposed to satisfy the cables' collision restrictions. The designed controller is an optimal controller using feedback linearization with optimized gains [10]. Afterward in [11] the same cable robot was promoted to a mobile cable robot by adding two actuators to the robot chassis (ICaSbot). Due to the non-holonomic structure of the robot, Gibbs-Appell equations were used to derive the related dynamic equations. Considering the internal dynamics of the system, linearized input-output feedback was used to control the robot. It should be noted that this robot also has a single-stage platform.

As mentioned, most previous research is related to single-stage space cable robots; Considering the superiority of the dual-stage space cable robot toward increasing the workspace of load transportation, dual stage is studied. There are few studies corresponding to dual-stage space cable robots in the literature. Contributed to this fact that the ability to manage and control the load is possible using dual-stage cable robots within the larger workspace, makes them the focus of attraction. Moreover, proper placement of the middle platform can result in a more optimized cables' tension distribution, and consequently, the extraction of optimal path, or increasing the load-carrying capacity can be accomplished in a more efficient way. Agrawal et al. tested a new dual-stage cable robot with two moving platforms connected in a series of parallel connections [12]. The robot is supposed to be employed in ships and considering the ocean conditions as a disturbance, a robust controller is implemented. Since the main

task of controlling the final operator is to move the load toward the target, the orientation of the middle platform is ignored and the system redundancy is added. In [13] kinematics and dynamics of this dual-stage robot, considering its special linking extracted and robust control of (Sliding Mode Control) SMC are designed and implemented. However, the optimization and determination of the DLCC of this robot are ignored in this research. In this article, the above-mentioned dual-stage robot is used for the generation of new trajectories to avoid the obstacle avoidance of the load and provide smooth movement. The first platform is employed for large movements while the second platform provides the accurate adjustment of the container. In the linking provided for this robot, the two platforms are coupled and all the motors are located on the fixed platform. Shafei et al. [14] presented a new control strategy for managing non-linear systems in the presence of mismatched uncertainties. In order to control the system in a robust and optimal way, a hybrid control system based on disturbance observer was developed, in which the optimal control is extracted according to State-dependent Riccati Equation approach while the robustness is provided based on second-order sliding mode.

This paper is dedicated to determine the load-carrying capacity for a dual-stage cable robot while its end-effector is tracking a predefined trajectory with the aid of an optimal closed-loop controller. Due to the possible changes in the transmission load as well as the no-load return, the system is exposed to uncertainty. Thus, the performance of the controller is investigated and the maximum DLCC is also calculated with and without this uncertainty. To meet this goal, the kinematics and dynamics of the dual-stage robot are extracted; Then, the state space equations are developed in the quasi-linear form to implement the State-Dependent Riccati equation controller (SDRE). Finally, the DLCC is calculated in the closed loop way according to the proposed flowchart and the presented restrictions. It is shown that using the suggested dual platform together with the presented SDRE optimal controller can significantly increase the load-transferring capability of the cranes.

2. Kinematic Modeling

The overall scheme of the proposed dual-stage

cable robot can be seen in Figure (1). The kinematic chain of a dual-stage cable robot is shown consisting of three A, B, and the final operator C platforms. Platforms B and C are connected to platform A by 12 cables. In general form, the platform A can be considered as a moving chassis.

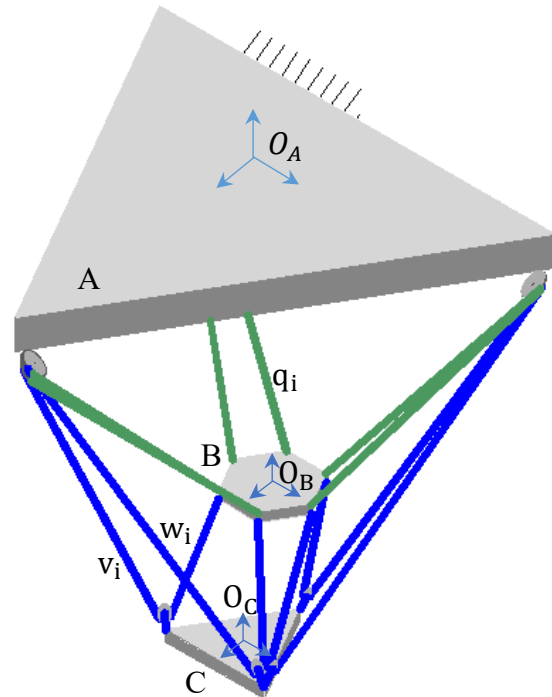


Fig.1. Dual-stage cable robot

On platform A, there are 12 motors, 6 of which control the movement of platform B directly using 6 cables, and the other 6 motors are connected to platform C by cables and the pulleys located on platform B. The orientation of each platform can be extracted using the rotational matrices relative to the inertia frame A in the form of Equation (1).

$${}^A\bar{x}_B = {}^A R_B(\psi_B, \theta_B, \varphi_B) \cdot {}^B\bar{x}_B \quad (1)$$

Where ${}^A R_B$ is rotation matrix of moving platform with respect to the base platform using a fixed axis rotation sequence of ψ , θ and φ about moving platform axes. Unit vectors of roll, pitch, and yaw which are defined in local coordinates are transferred to the global coordinates. Thus, the angular velocity of frames B and C with respect to A can be defined in their related frames while their global values can be extracted by transferring the data to the global coordinates (A) using the corresponding rotational matrices. The angular velocity of platform B with respect to the inertial coordinate A can be obtained in

Equation (2).

$${}^B\omega_{BA} = \begin{bmatrix} \omega_{b1} \\ \omega_{b2} \\ \omega_{b3} \end{bmatrix} = \begin{bmatrix} 1 & 0 & -S\theta_b \\ 0 & C\psi_b & S\psi_b C\theta_b \\ 0 & -S\psi_b & C\psi_b C\theta_b \end{bmatrix} \begin{bmatrix} \dot{\psi}_b \\ \dot{\theta}_b \\ \dot{\phi}_b \end{bmatrix} \triangleq P_b \cdot \dot{\Psi}_b \quad (2)$$

where ω_{bi} is the angular velocity of platform B around the principal axes in local coordinate.

Therefore, the angular velocity and acceleration of platform C can be obtained relative to the inertial reference A. Cable tension vectors are defined as the multiplication of the tension values of each cable by its related unit vector. Generally, the length of the cables Eq. (3) is a function of the position and orientation of frames B and C, therefore;

$$l_i(\underline{X}) = l_i(x_B, y_B, z_B, \psi_B, \theta_B, \varphi_B, x_C, y_C, z_C, \psi_C, \theta_C, \varphi_C) \quad (3)$$

Where three translational components and three orientational ones of each platform, (\underline{X}) , are considered. In this equation, Jacobian is defined as Equation (4);

$$J = \left[\frac{\partial l}{\partial \underline{X}} \right] \quad (4)$$

The fixed platform (A) and moving platforms (B and C) are shown in Figure (2). In addition, the configuration of cables' connections to the platforms is given in Eq. (5).

$$\begin{cases} \vec{q}_1 = \overrightarrow{B_2A_1} & \vec{q}_2 = \overrightarrow{B_2A_2} & \vec{q}_3 = \overrightarrow{B_4A_2} \\ \vec{q}_4 = \overrightarrow{B_4A_3} & \vec{q}_5 = \overrightarrow{B_6A_3} & \vec{q}_6 = \overrightarrow{B_6A_1} \\ \vec{v}_1 = \overrightarrow{C_1A_1} & \vec{v}_2 = \overrightarrow{C_1A_2} & \vec{v}_3 = \overrightarrow{C_2A_2} \\ \vec{v}_4 = \overrightarrow{C_2A_3} & \vec{v}_5 = \overrightarrow{C_3A_3} & \vec{v}_6 = \overrightarrow{C_3A_1} \\ \vec{w}_1 = \overrightarrow{C_1B_3} & \vec{w}_2 = \overrightarrow{C_2B_3} & \vec{w}_3 = \overrightarrow{C_2B_5} \\ \vec{w}_4 = \overrightarrow{C_3B_5} & \vec{w}_5 = \overrightarrow{C_3B_1} & \vec{w}_6 = \overrightarrow{C_1B_1} \end{cases} \quad (5)$$

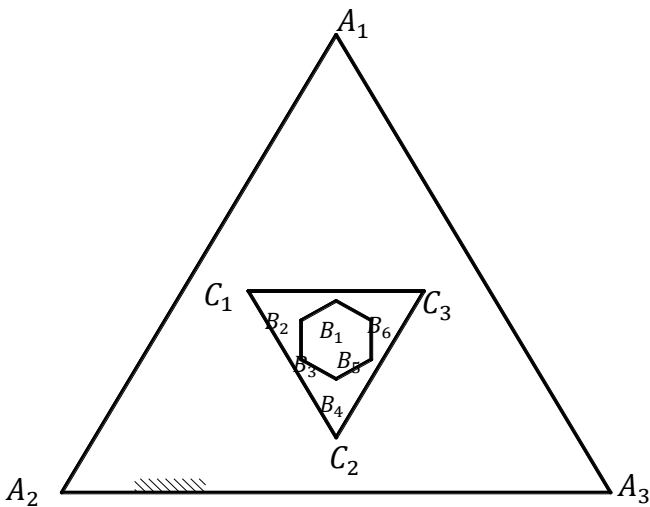


Fig.2. The configuration of the cables' connections to the platforms

According to Figure (3), the length of the cables can be obtained according to the rules of the vector. The q_i cables connect the intermediate platform to the fixed one, the v_i cables connect the end effector to the fixed platform, and the w_i cables connect the end effector to the intermediate platform.

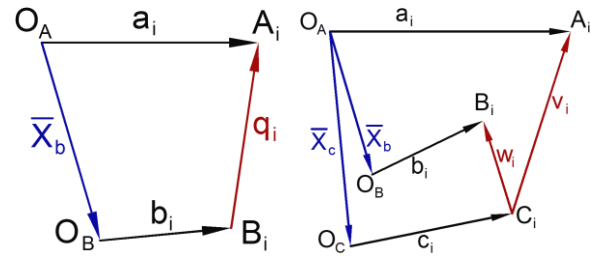


Fig.3. a) Cables q b) Cable v and w

where X is the position vector of the center of the platforms relative to platform A. Vectors b and c are the vectors of connection points to the platforms with respect to the local coordinates. Since the cables v and w are connected by pulleys and their total length is controlled by a motor, they are essentially considered as one cable, so;

$$l_i(\underline{X}) = \begin{cases} q_i(\underline{X}) & i = 1:6 \\ v_{i-6}(\underline{X}) + w_{i-6}(\underline{X}) & i = 7:12 \end{cases} \quad (6)$$

3. Dynamic Formulation

The dynamic equations of the dual-stage cable robot are obtained for moving chassis using Newton-Euler method [13].

$$M(\underline{X})\ddot{\underline{X}} + F(\underline{X}, \dot{\underline{X}}) + D(\underline{X}) = J(\underline{X})T$$

$$M(\underline{X}) = \begin{bmatrix} M_b & O_3 \\ O_3 & M_b \end{bmatrix}, \quad F(\underline{X}, \dot{\underline{X}}) = \begin{bmatrix} F_b \\ F_c \end{bmatrix}$$

$$D(\underline{X}) = \begin{bmatrix} D_b \\ D_c \end{bmatrix}, \quad J(\underline{X}) = \begin{bmatrix} J_b \\ J_c \end{bmatrix} \quad (7)$$

where M is the matrix of inertia, F is the Coriolis and Centrifugal force vector and D is the gravity vector. Considering the chassis as a fixed plate, the dynamic equations for each frame B and C are in the form of Equations (8) and (9).

$$\begin{bmatrix} m_b I_3 & O_3 \\ O_3 & {}^A R_B I_b P_b \end{bmatrix} \begin{bmatrix} \ddot{x}_b \\ \dot{\Psi}_b \end{bmatrix} + \begin{bmatrix} O_{3 \times 1} \\ F_{O,b} \end{bmatrix} + \begin{bmatrix} -m_b \vec{g} \\ O_{3 \times 1} \end{bmatrix} = \begin{bmatrix} \vec{q}_1/q_1 & \dots & -\vec{w}_6/w_6 \\ {}^A R_{b1} \times \vec{q}_1/q_1 & \dots & -{}^A R_{b12} \times \vec{w}_6/w_6 \end{bmatrix} T \quad (8)$$

$$\begin{bmatrix} m_c I_3 & O_3 \\ O_3 & {}^A R_C I_c P_c \end{bmatrix} \begin{bmatrix} \ddot{x}_c \\ \dot{\Psi}_c \end{bmatrix} + \begin{bmatrix} O_{3 \times 1} \\ F_{O,c} \end{bmatrix} + \begin{bmatrix} -m_c \vec{g} \\ O_{3 \times 1} \end{bmatrix} = \begin{bmatrix} \vec{v}_1/v_1 & \dots & \vec{w}_6/w_6 \\ {}^A R_{c1} \times \vec{v}_1/v_1 & \dots & {}^A R_{c12} \times \vec{w}_6/w_6 \end{bmatrix} T \quad (9)$$

Where;

$$F_{O,b} = {}^A R_B I_b \dot{P}_b \Psi_b + {}^A R_B P_b \Psi_b \times {}^A R_B I_b P_b \Psi_b \quad (10)$$

Due to the fact that changes in spatial components

do not affect the Coriolis and Centrifugal forces, the vector of these forces, which is only affected by changes in angular components, is called $F_{O,b}$ and $F_{O,c}$. also m_b and m_c are masses of the engaged platforms, and I_b and I_c are their related rotational inertia. The vector of the motors' torque Eq. (11) can be obtained by adding the motor dynamics to platform one as follows:

$$\tau = r \cdot J(\underline{X})^{-1} \left(M(\underline{X}) \ddot{\underline{X}} + F(\underline{X}, \dot{\underline{X}}) + D(\underline{X}) \right) + j \cdot \left(\frac{d}{dt} \left(\frac{\partial \beta}{\partial \underline{X}} \right) \dot{\underline{X}} + \frac{\partial \beta}{\partial \underline{X}} \ddot{\underline{X}} \right) + c \cdot \left(\frac{\partial \beta}{\partial \underline{X}} \dot{\underline{X}} \right) \quad (11)$$

where j , c , and r are the rotational moment inertia of the rotor and pulleys, the damping coefficient of the electromotor, and the radius of the pulleys, respectively. These parameters are selected equally for all motors simplifying the calculations without reducing the overall work. In this equation, the vector β is related to the rotation angle of the motors.

4. SDRE Controller and Quasi-Linear Equation

The state-dependent Riccati Equation is one of the most powerful optimization tools since it can optimally control the dynamics of a system in a nonlinear and closed-loop way. In this method, nonlinear dynamic equations are rewritten in a quasi-linear structure, so that the use of optimal linear control methods could be possible. After solving the Hamilton-Jacobi-Bellmann equation, the state matrix appearing in the Riccati equation will no longer be constant and will be considered as a function of the system state variables and this is the only existing difference. The optimal feedback gain is obtained and the stability and optimality of the response can be achieved simultaneously by solving this Riccati algebraic equation at any moment. It can be stated that the SDRE is a kind of DI for which the feedforward terms are added and the feedback gains are tuned automatically using the defined cost function. It is worth mentioning that in nonlinear conditions, there is nonlinearity in the controller input. The problem with this type of nonlinearity is the complexity of the numerical calculations which needs to be solved in the SDRE controller. Thus, in most proposed methods, the system is optimized in offline mode. In such systems, the states are nonlinear. If the linear relationship between the input vector and the system states is established, the system equation can be written as

Equation (12) [16];

$$\dot{\underline{x}} = f(\underline{x}) + B(\underline{x})u \quad (12)$$

Considering the combined dynamic equations of the robot and the actuators (Eq. (11)), the controllers must be quasi-linear to use these equations in the SDRE controller [17]. By rewriting this formula in terms of the first and second derivatives of the variables, Equation (13) is obtained.

$$\left[M + J \frac{j}{r} \left(\frac{\partial \beta}{\partial \underline{X}} \right) \right] \ddot{\underline{X}} + \left[J \frac{j}{r} \frac{d}{dt} \left(\frac{\partial \beta}{\partial \underline{X}} \right) + J \frac{c}{r} \left(\frac{\partial \beta}{\partial \underline{X}} \right) \right] \dot{\underline{X}} + F + D = \frac{1}{r} J \tau \quad (13)$$

Or simply,

$$\tilde{M} \ddot{\underline{X}} + \tilde{N} \dot{\underline{X}} + F + D = \frac{1}{r} J \tau \quad (14)$$

Now, the 12 second-order differential equations are converted to 24 first-order equations. The arrangement of the state vectors is chosen as Equation (15);

$$\underline{Z}(t) = \{x_B(t), y_B(t), \dots, x_C(t), y_C(t), \dots, \dot{x}_B(t), \dot{y}_B(t), \dots, \dot{x}_C(t), \dot{y}_C(t), \dots\} \quad (15)$$

or,

$$\underline{q}(t) = \{q_1(t), q_2(t), \dots, q_{12}(t), \dot{q}_1(t), \dot{q}_2(t), \dots, \dot{q}_{12}(t)\} \quad (16)$$

Then, the state equations can be obtained as Equation (17).

$$\begin{cases} \dot{q}_i(t) = q_{i+12}(t) \\ \dot{q}_{i+12}(t) = \tilde{M}^{-1} (-\tilde{N} q_{i+12}(t) - F - D) + \tilde{M}^{-1} \left(\frac{1}{r} J \right) \tau \end{cases} \quad I=1:12 \quad (17)$$

Equation (17) should be written in quasi-linear form Equation (18) to be applicable in SDRE controller,

$$\dot{\underline{X}}(t) = A(\underline{X})\underline{X}(t) + B(\underline{X})u(t) \quad (18)$$

The goal is to reach a stabilizing control u while minimizing the cost function J of Eq. (19);

$$J(x_0, u(0)) = \frac{1}{2} x(T)^T P(T) x(T) + \frac{1}{2} \int_0^T \{x^T(t) Q(x) x(t) + u^T(t) R(x) u(t)\} dt \quad (19)$$

$Q(x) \geq 0, R(x) \geq 0, P(T) \geq 0$

where $Q(x)$ is the gain matrix of accuracy and $R(x)$ is the gain matrix of control input. The state weighting matrices and the input are assumed to be a function of the state variable. This is another advantage of SDRE controllers weighting matrices can be designed to increase $Q(x)$ and decrease $R(x)$ by increasing the state variable. This type of design results in maintaining a control effort near a predetermined path. The control rule can be obtained then as a closed loop formula of Equation (20) for which the cost function is approximately minimum.

$u(X) = -K(X)\underline{X}(t) = -R^{-1}(X)B^T(X)P(X)\underline{X}(t)$ (20)
 Here $P(x)$ should be extracted using the following state-dependent Eq. (21).

$$P(X)A(X) + A^T(X)P(X) - P(X)B(X)R^{-1}(X)B^T(X)P(X) + Q(X) = 0 \quad (21)$$

$P(x)$ is a symmetric and positive definite matrix. Finally, the quasi-linear matrix A is obtained as Equation (22) if the equation would be written as a matrix and quasi-linear form.

$$A = \begin{bmatrix} O_{12 \times 12} & I_{12 \times 12} \\ \tilde{D}_{12 \times 12} & \tilde{F}_{12 \times 12} - \tilde{M}^{-1} \cdot \tilde{N} \end{bmatrix} \quad (22)$$

Where;

$$\tilde{F} = \begin{bmatrix} O_{3 \times 3} & O_{3 \times 3} & O_{3 \times 3} & O_{3 \times 3} \\ O_{3 \times 3} & F_B & O_{3 \times 3} & O_{3 \times 3} \\ O_{3 \times 3} & O_{3 \times 3} & O_{3 \times 3} & O_{3 \times 3} \\ O_{3 \times 3} & O_{3 \times 3} & O_{3 \times 3} & F_C \end{bmatrix} \quad (23)$$

and,

$$\tilde{D} = \begin{bmatrix} 0 & 0 & 0 & 0 \\ 0 & 0 & 0 & \dots & 0 \\ 0 & 0 & -m_b g / z_B & 0 \\ & \vdots & & \ddots & \vdots \\ 0 & 0 & 0 & \dots & 0 \\ 0 & 0 & 0 & \dots & 0 \\ 0 & 0 & 0 & \dots & 0 \end{bmatrix} \quad (24)$$

The quasi-linear input matrix can be selected as Equation (26).

$$B(X) = \begin{bmatrix} O_{12 \times 12} \\ \tilde{B}(X) \end{bmatrix} \quad (25)$$

$$\tilde{B}(X) = \left[M - J \frac{j}{r} \left(\frac{\partial \beta}{\partial X} \right) \right]^{-1} \cdot \left(\frac{J}{r} \right) \quad (26)$$

The algorithm of the proposed controlling strategy is shown in Figure (4).

5. Load Carrying Capacity

Determining the load-carrying capacity is essential when the system is tracking a predefined path. The main constraints of the robot dynamics include positive tension of the cables and cables' interference avoidance. Thus, the load replacement should be conducted within a predefined path

for which the mentioned constraints could be satisfied. To do so, the maximum motor torque and the maximum allowable deviation of the actuators from their related path should be considered. Therefore, coefficients for evaluating and modeling the motor torque restrictions and their accuracy need to be calculated. In [15] two groups of dimensionless coefficients are defined as torque coefficients (C_a) and accuracy coefficient (C_p), according to the robot dynamics, the motor's torque and allowable errors of the end effector along the predefined path.

$$C_a = \min \left\{ \frac{\tau_{ai}}{\max\{|r|^{-1}(\tilde{M}\underline{X} + \tilde{N}\underline{X} + F + D)\}_i - \max\{\tau_{ni}\}}, = 1..12 \right\} \quad (27)$$

$I = 1.12$
 the τ_{ai} is the maximum allowable torque to increase for each motor at any point in the path. τ_{ni} is the calculated torque for free-load motors, and only the weight of the final operator and the middle platform are considered in these calculations.

$$C_p = \frac{e_w}{e_a} = \frac{e_w}{\|X_a(t) - X_d(t)\|} \quad (28)$$

where $X_a(t)$ and $X_d(t)$ show the actual and desired position of the final operator and e_w is the controller fault, respectively. The iterative method like the flowchart presented in Figure 5, was presented to find the DLCC of a robot based on torque and error constraints. According to the definition, the maximum value of these coefficients is 1 and occurs if one of the motors is saturated at one of the points or the position of the operator in the unauthorized area is off regarding the path.

6. Dual-Stage Cable Robot Validation

To verify the correctness of the modeling, the performance of the robot through the simulation is compared with the performance of the ICaSbot single-stage cable space robot (Fig. 6).

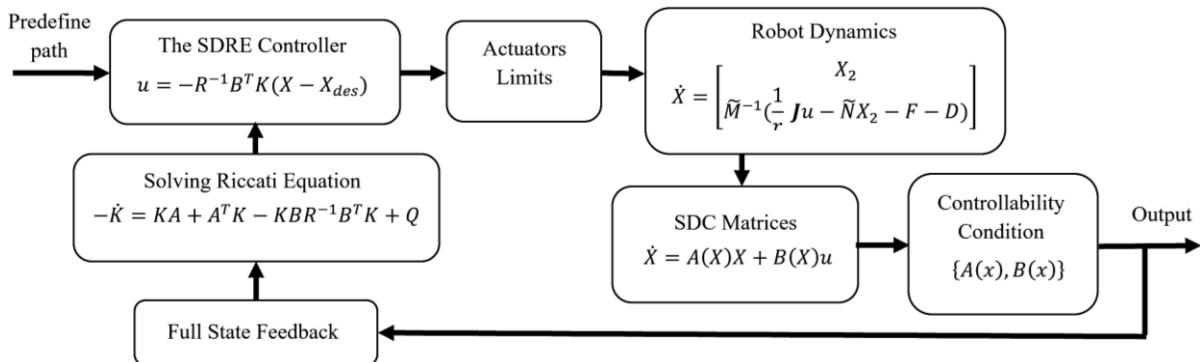


Fig.4. Real-time SDRE controller flowchart

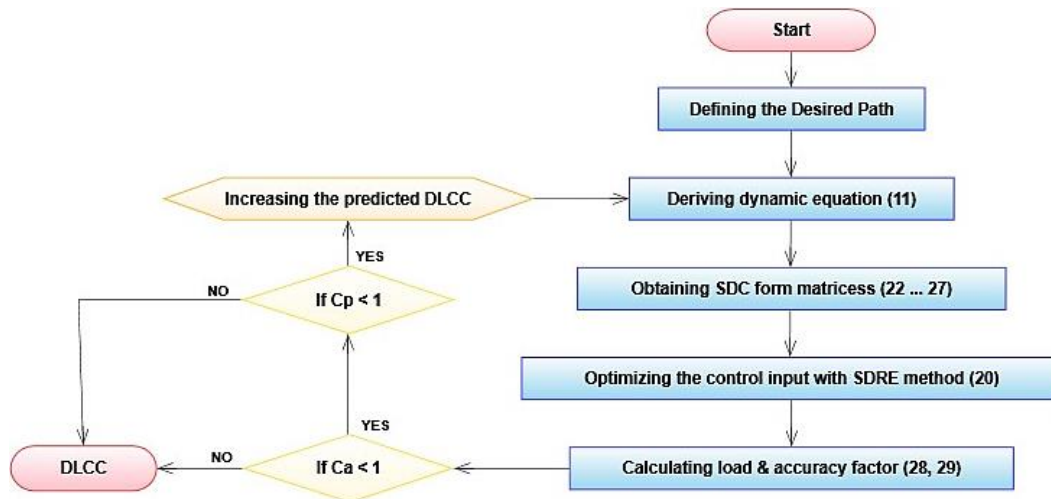


Fig.5. Flowchart for calculating the dynamic load-carrying capacity for a given trajectory

To make the compatibility of the presented dual-stage cable robot with the mentioned single stage one [14], the middle platform is attached to the end-effector of the robot at a negligible distance. Zero distance is not possible since the Jacobian matrix will be singular. In other words, if the distance between the intermediate platform and the end-effector tends to zero, then one can conclude that the presented dual stage cable robot tends to single-stage one. Moreover, the shape and dimensions of this platform are considered roughly the same size as the dimensions of the end-effector. In this case, the mobility of both platforms can be defined by a unique function, and its mass and moment of inertia are neglected compared to the end-effector's.



Fig.6. Space cable robot (ICaSbot)

The end-effector weight is 1.09 kg and the load is 0.5 kg. The predetermined path is also a circular

path at a distance of 45 cm below the fixed platform. The performance of both types of robots against 50% uncertainty is shown in Figure (7). In this simulation, in addition to validating the modeling, the performance of the SDRE controller can be observed in comparison with the optimal LQR controller [15]. The similar response of the open-loop diagrams shown in parts a and b of Figure (7) shows the correctness of the two-stage spatial cable robot modeling. On the other hand, it can be seen that the SDRE controller performance (part b) has a significantly better response compared to the optimal LQR controller. To compare the torques, a payload of 3.4 kg (Compared with 0.5 kg in [15]) was chosen. As can be seen from Figure 8, the trends of the curves are generally similar. Differences are contributed to the fact that additional actuating cables are engaged. Also, due to the difference between the two controllers (LQR for single stage vs. SDRE for dual), the response speed is a little bit different.

Considering the fact that the main superiority of dual cable robots is their larger rotational movement, another simulation scenario is considered here in which the platforms have also rotational movement. The path and changes of the cables' length for the movements of Equations (30, 31) is studied here.

$$t < 10 \text{ s} \longrightarrow \begin{cases} x_c = 0.05 \cos\left(\frac{\pi t^2}{100}\right) \\ y_c = 0.05 \sin\left(\frac{\pi t^2}{100}\right) \\ z_c = -0.45 \\ \psi_c = 0.03 \sin\left(\frac{\pi t}{2}\right) \\ \theta_c = 0 \\ \varphi_c = 0 \end{cases} \quad (29)$$

$$10\text{ s} < t < 20\text{ s} \rightarrow \begin{cases} x_c = 0.05 \cos\left(\frac{\pi(t-20)^2}{100}\right) \\ y_c = -0.05 \sin\left(\frac{\pi(t-20)^2}{100}\right) \\ z_c = -0.45 \\ \psi_c = 0.03 \sin\left(\frac{\pi t}{2}\right) \\ \theta_c = 0 \\ \varphi_c = 0 \end{cases} \quad (30)$$

To study the effect of rotational movement of the platforms on the kinematics and kinetics of the robot, the comparison of the robot DOFs for circular movement between fixed platforms' angle and variable angle modes (Figure (9a, 9b)), comparison of cables' length (Figure (9c, 9d)) and comparison of motors' torque (Figure (9e, 9f)) are

shown. It can be seen that both the kinematic and kinetic profiles have a little increase in amplitude with higher distortion compared to fixed mode which is the result of the harmonic movement of the platform pitch. Therefore, the trajectory will have a significant impact on determining the DLCC.

7. Simulation

In the simulation performed for a dual-stage cable robot with six degrees of freedom and six degrees of cable redundancy, the following dimensional specifications have been considered:

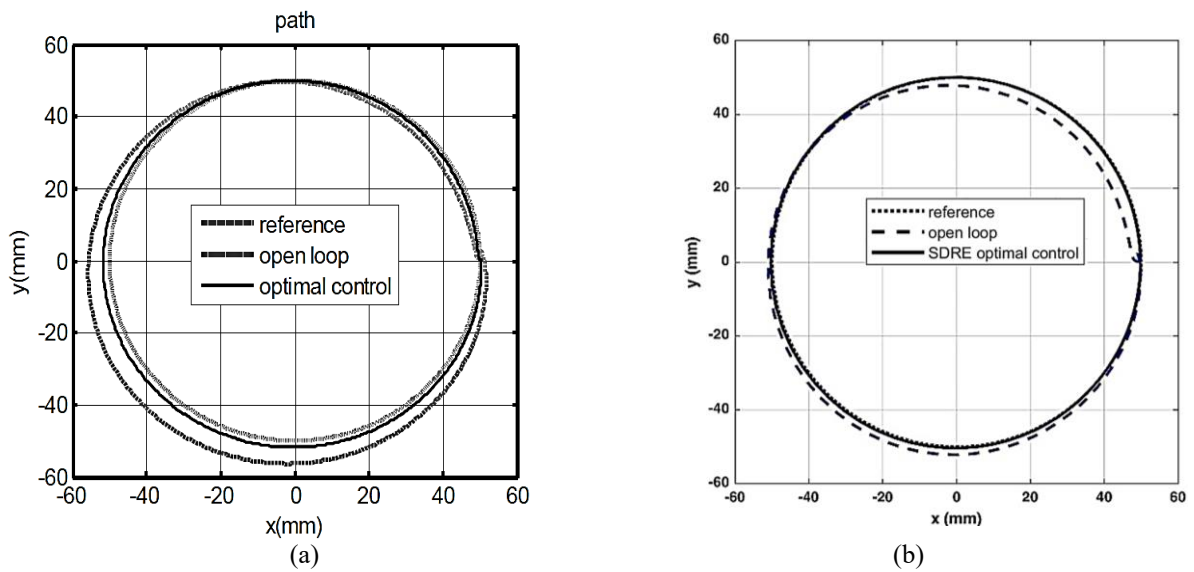


Fig.7. Comparison of the path traveled by the system equipped with the controller and the open loop system in both (a) single-stage (b) and dual-stage robot

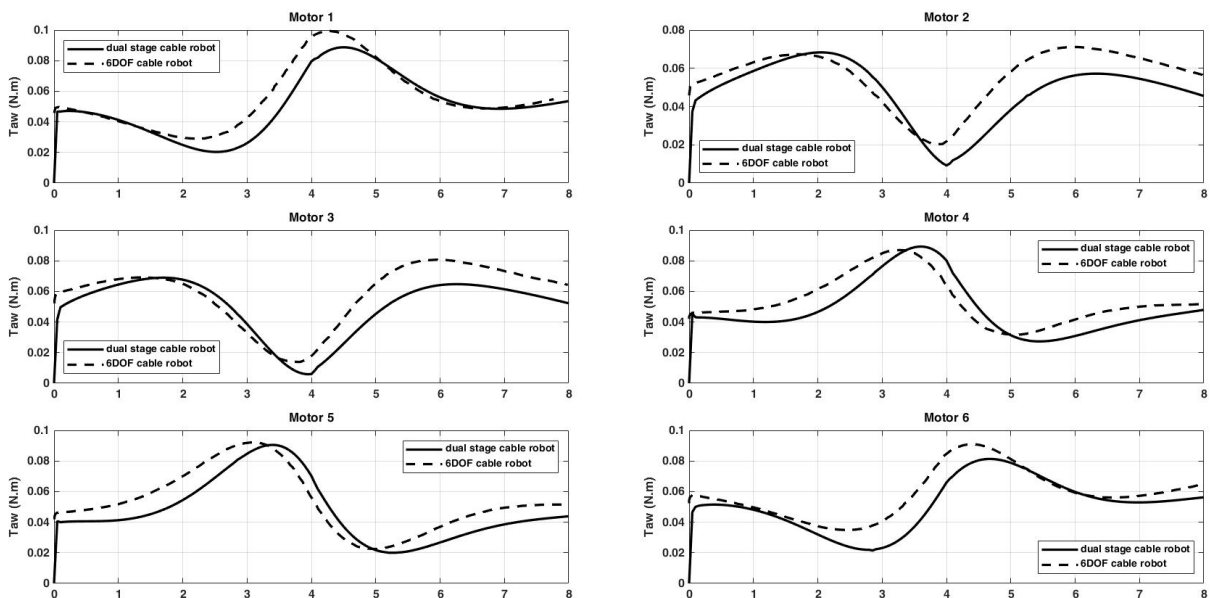


Fig.8. Comparison of the motors torque profiles for dual-stage cable robot and single-stage cable robot

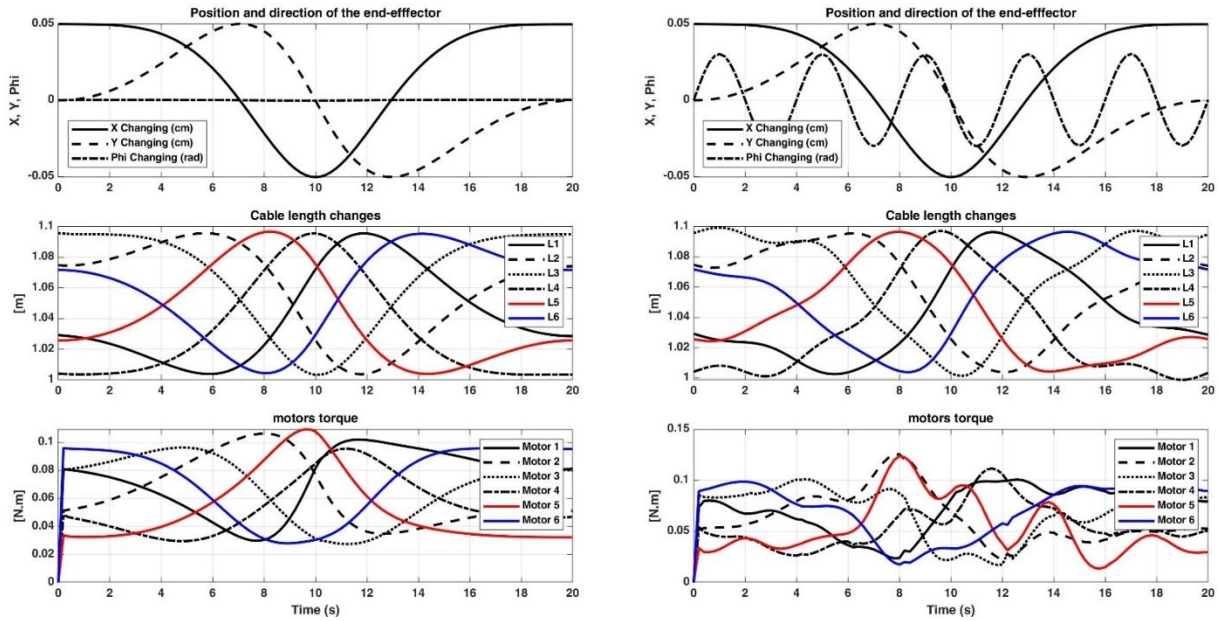


Fig.9. Comparison of the DOFs, motor's torque, and length of the cables connected to the end-effector in circular motion with fixed and variable pitch angle

Tab.1. Characteristics of the spatial dual cable robot

Title	Symbol	Ratio	Unit
Moment of inertia of the end-effector	I_C	$I_{Cxx} = I_{Cyy} = 0.0018, I_{Czz} = 0.0036$	kg. m ²
Moment of inertia of the middle platform	I_B	$I_{Bxx} = I_{Byy} = 0.0002, I_{Bzz} = 0.0004$	kg. m ²
Mass of the end-effector	m_C	1.09	kg
Middle platform weight	m_B	0.1	kg
Size and dimensions of the fixed platform*	r_A	0.68	m
Size and dimensions of the middle platform*	r_B	0.05	m
Size and dimensions of the end-effector*	r_C	0.098	m
The pulley radius of the motor	r	0.015	m
The damping coefficient of the motor	c	0.01	N. m/rad
Rotational inertia of the motor	j	0.0008	kg. m ²
Error gain matrix	Q	diag(100)	—
Input gain matrix	R	diag(0.1)	—
Stall torque of the motors	τ_s	300	N.mm
The free running speed of the motors	ω_0	286.5	RPM

- The radius of the circumference circle on the platform panel

In this part, to determine the load-carrying capacity of the dual robot and also to increase the load-carrying capacity through the proportional distribution of the cable tension, the following simulation is performed.

In all cases, the predefined path for the end-effector is a circular path with zero initial velocity which increases linearly. Then, in the middle of the path with a constant negative acceleration, the speed decreases to zero. Initially, the middle platform is located at a height of 20 cm lower than the fixed platform and remains fixed during the end-effector's path. It should be noted that in this simulation the middle platform

is fixed.

Figure 10 shows the torque saturation diagram of the actuators for two types of single and two-stage robots. In a single-stage robot with a DLCC of 4.5 kg, the motors have reached the saturation state [14], while in a two-stage robot, the related maximum DLCC is 10.5 kg, which is more than double. In both types, the load factor is saturated and the accuracy factor remains within the specified allowable range ± 1 mm (Fig. 11).

To check the performance of the dual robot SDRE controller, all DLCC can be considered as uncertainty, which may occur in practice.

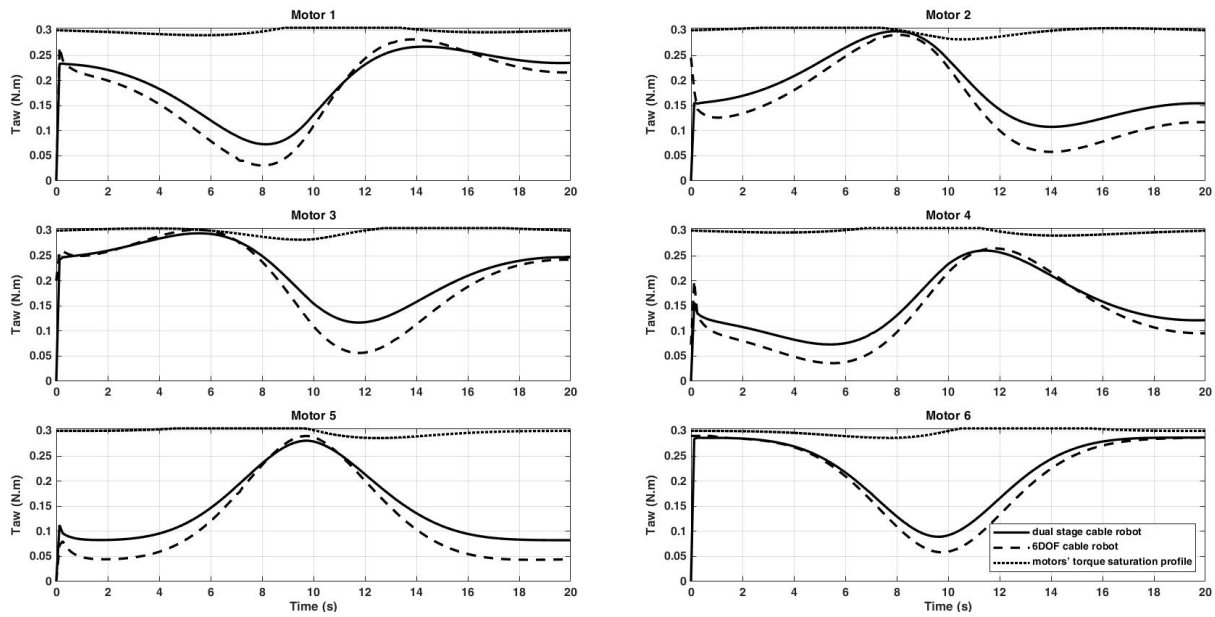


Fig.10. Comparison of motors torque saturation profiles for dual-stage cable robot and single-stage cable robot

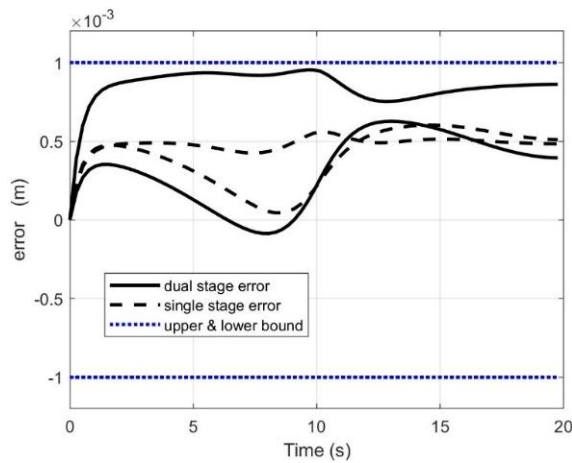


Fig.11. Comparison of the error along the x and y axes for the dual and single-stage cable robot

In Figure 12, for the applied load uncertainty, the accuracy factor is not saturated and the error remains within the allowed range for the closed-loop system, while for the open-loop system with 0.3 kg of uncertainty payload, the accuracy factor is saturated. This robustness shows the efficiency of the proposed closed-loop nonlinear controller for this dual-stage cable robot.

Another advantage of the proposed dual-stage cable robot is its over-actuated entity which enables us to choose different paths for a unique destination toward increasing the DLCC. The payload of the end-effector can be increased by moving the intermediate platform, in proportion to the end-effector, since the cable's tensions

can be distributed in a more optimized way. In Figure 13, by considering a circular motion for the intermediate platform synchronous with the end-effector, 12.4 kg payload can be carried by which the torque is saturated and cable interference constraint is also satisfied. However, this amount of load does not indicate the DLCC since the accuracy constraint must be also controlled.

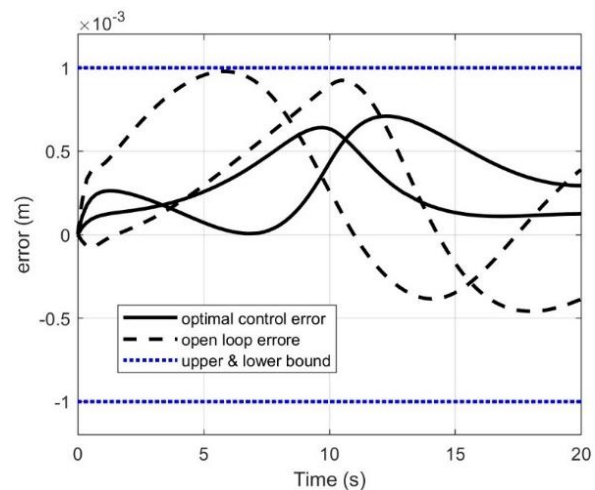


Fig.12. Comparison of the error along the x and y axes for the open-loop and the optimal closed-loop SDR controller

By checking the accuracy conditions, it is clear that the payload is violated and therefore the payload should be reduced.

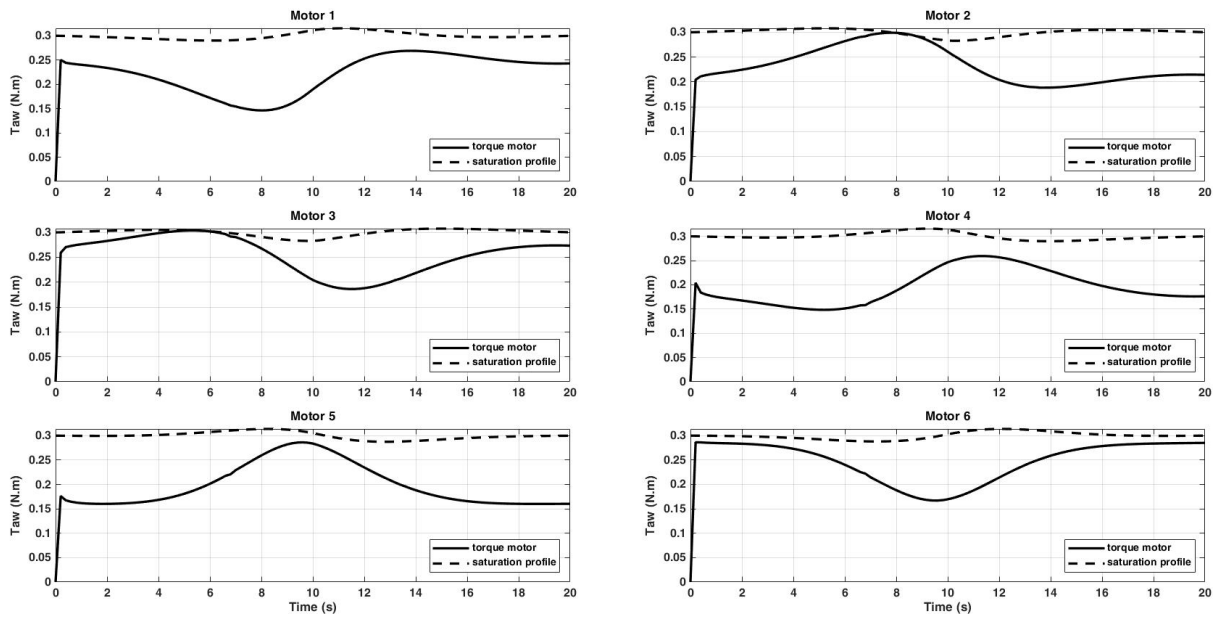


Fig.13. Motors torque saturation profiles with 12.4 kg payload

By performing the mentioned iteration algorithm, to meet the accuracy condition (Fig. 14), the amount of carrying capacity for this condition will be 11.8 kg.

It can also be seen that by changing the path of the middle platform, the cables' tension changes are reduced which eventually leads the system to have a higher DLCC. In this way, by adjusting the position of the middle platform, the tension of the cable can be controlled and its tension can be prevented from becoming zero, which in turn expands the workspace of the robot.

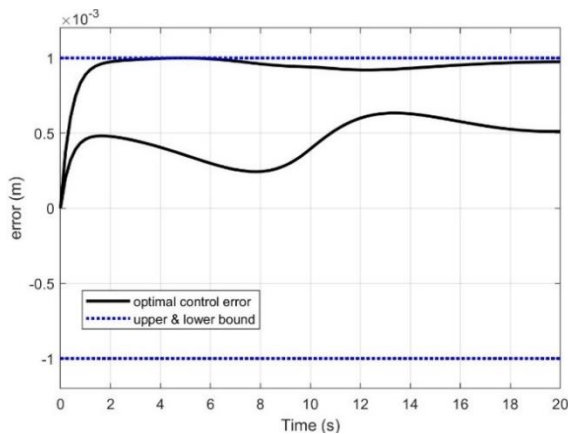


Fig.14. Error along the x and y axes with 11.8 kg DLCC

8. Conclusion

In this paper, the dynamic load-carrying capacity for a dual-stage space cable robot is obtained

based on an iterative algorithm and employing an optimal SDRE approach. The constraints used to determine the DLCC in this algorithm were accuracy and motor torque. The kinematics and dynamics of the robot were derived with six degrees of cable redundancy. SDRE controller was used to increase the accuracy of the robot for load transfer in the predetermined path. In addition, load uncertainty was used to show the efficiency of the controller. It was seen that the controller can handle the end-effector in both of translational and rotational movement in the presence of 900% uncertainty on the load parameter. It was seen that the maximum DLCC of the dual-stage cable robot with SDRE controller is 10.5 kg, thanks to double number of the engaged motors which is 16.7% higher than the single stage robot. It was also shown that by moving the middle platform, in addition to controlling the tension of the cables and preventing them from becoming zero, the load carrying capacity can be increased. Thus, it can be concluded that the presented robot with the designed controller can be used for object handling of heavy load for large workspace conditions.

Reference

[1]. R. Bostelman, J. Albus, N. Dagalakis, A. Jacoff, and J. Gross, "Applications of the NIST RoboCrane", in Proceedings of the 5th International Symposium on Robotics

- and Manufacturing, vol. 5, 1994, p. 1.
- [2]. R. Verhoeven, "Analysis of the workspace of tendon-based Stewart platforms". Duisburg, Essen, Univ., Diss., 2006.
- [3]. A. B. Alp and S. K. Agrawal, "Cable suspended robots: design, planning, and control", in Proceedings IEEE International Conference on Robotics and Automation (Cat. No. 02CH37292), vol. 4, 2002, pp. 4275–4280.
- [4]. J. Pusey, A. Fattah, S. Agrawal, and E. Messina, "Design and workspace analysis of a 6–6 cable-suspended parallel robot", Mech. Mach. Theory, vol. 39, no. 7, 2004, pp. 761–778.
- [5]. S.-R. Oh, J.-C. Ryu, and S. K. Agrawal, "Dynamics and control of a helicopter carrying a payload using a cable-suspended robot", 2006.
- [6]. W. Lv, L. Tao, and Z. Ji, "Sliding mode control of cable-driven redundancy parallel robot with 6 DOF based on cable-length sensor feedback", Math. Probl. Eng., vol. 2017, 2017.
- [7]. J. Lamaury, M. Gouttefarde, A. Chemori, and P.-E. Hervé, "Dual-space adaptive control of redundantly actuated cable-driven parallel robots", in IEEE/RSJ International Conference on Intelligent Robots and Systems, 2013, pp. 4879–4886.
- [8]. G. Mottola, C. Gosselin, and M. Carricato, "Dynamically feasible motions of a class of purely-translational cable-suspended parallel robots", Mech. Mach. Theory, vol. 132, 2019, pp. 193–206.
- [9]. M. H. Korayem and M. Bamdad, "Dynamic load-carrying capacity of cable-suspended parallel manipulators", Int. J. Adv. Manuf. Technol., vol. 44, no. 7, 2009, pp. 829–840.
- [10]. M. H. Korayem, M. Bamdad, H. Tourajizadeh, H. Shafiee, R. M. Zehtab, and A. Iranpour, "Development of ICASBOT: cable-suspended robots with Six DOF", Arab. J. Sci. Eng., vol. 38, no. 5, 2013, pp. 1131–1149.
- [11]. M. H. Korayem, M. Yousefzadeh, and S. Manteghi, "Dynamics and input-output feedback linearization control of a wheeled mobile cable-driven parallel robot", Multibody Syst. Dyn., vol. 40, no. 1, 2017, pp. 55–73.
- [12]. S.-R. Oh, K. Mankala, S. K. Agrawal, and J. S. Albus, "A dual-stage planar cable robot: dynamic modeling and design of a robust controller with positive inputs", 2005.
- [13]. S.-R. Oh, K. K. Mankala, S. K. Agrawal, and J. S. Albus, "Dynamic Modeling and Robust Controller Design of a Two-Stage Parallel Cable Robot", Multibody Syst. Dyn., vol. 13, no. 4, 2005, pp. 385–399.
- [14]. H. R. Shafie, M. Bahrami and, H. A. Talebi, "Disturbance observer-based two-Layer control strategy design to deal with both matched and mismatched uncertainties", Robust and Nonlinear Control, Vol. 31, Issue 5, 25 March 2021.
- [15]. M. H. Korayem and H. Tourajizadeh, "Maximum DLCC of spatial cable robot for a predefined trajectory within the workspace using closed-loop optimal control approach", J. Intell. Robot. Syst., vol. 63, no. 1, 2011, pp. 75–99.
- [16]. T. Çimen, "Systematic and effective design of nonlinear feedback controllers via the state-dependent Riccati equation (SDRE) method", Annu. Rev. Control, vol. 34, no. 1, 2010, pp. 32–51.
- [17]. S. R. Nekoo and B. Geranmehr, "Control of non-affine systems using the state-dependent Riccati equation (SDRE)", Majlesi J. Mechatron. Syst., vol. 2, no. 4, 2013.

Follow this article at the following site:

Mohsen Nourizadeh, Moharram Habibnejad Korayem, Hami Tourajizadeh.
 "Control Optimization of a Dual-Stage Cable Robot with Redundancy Using State
 Dependent Riccati Equation Approach" IJIEPR 2025; 36 (1): 159-170
 URL: <http://ijiepr.iust.ac.ir/article-1-2231-en.html>

